VIP Chiral Resolution Very Important Paper

How to cite:
International Edition: doi.org/10.1002/anie.202003807
German Editon: doi.org/10.1002/ange.202003807

Single-Layered Chiral Nanosheets with Dual Chiral Void Spaces for Highly Efficient Enantiomer Absorption

*Xiaopeng Feng, Bowen Shen, Bo Sun, Jehan Kim, Xin Liu, and Myongsoo Lee**

Abstract: *Although considerable effort in recent years has been devoted to the development of two-dimensional nanostructures, single-layered chiral sheet structures with a lateral assembly of discrete clusters remain elusive. Here, we report single-layered chiral 2D sheet structures with dual chiral void spaces in which discrete clusters of planar aromatic segments are arranged with in-plane AB order in aqueous methanol solution. The chirality of the sheet is induced by the slipped-cofacial stacks of rectangular plate-like aromatic segments in the discrete clusters which are arranged laterally with up and down packing, resulting in dual chiral void spaces. The chiral nanosheets function as superfast enantiomer separation nanomaterials, which rapidly absorb a single enantiomer from a racemic mixture with greater than 99 % ee.*

The construction of two-dimensional (2D) nanostructures is an attractive target owing to their unique properties for many promising applications in separation, energy storage, optoelectronics, and catalysis.[1–4] However, it remains a challenge to synthesize single-layered 2D sheet structures without using 2D templates, which are essential for the unique structural, mechanical, and electronic properties that make them highly attractive in many applications.[5–9] The single-layered sheets can be constructed by the self-assembly of multipod aromatic segments[10–12] or macrocycle amphiphiles,[13] and the exfoliation of metal–organic or covalent organic frameworks.[14–16] Despite such recent achievements in 2D materials, most of the 2D framework structures do not display properties for chiral recognition since such framework design encounters difficulties in breaking mirror symmetry in two dimensions. Stacks of flat objects twisted in one direction overcome this problem due to mirror symmetry breaking, as exemplified in the twist stacking of bilayer graphene.[17] Symmetry breaking by twisting can be applied to macrocycle stacks to generate chiral pores.[18] For example, when facing macrocycle dimers are twisted with respect to each other in one direction, the breaking of mirror symmetry induces the formation of chiral pores.[19] The twisted dimeric stacks with a chiral interior laterally associate to form single-layered chiral sheet structures, while layer stacks are prohibited because the 2D aromatic surfaces are covered by the flexible chains.

Another approach to 2D chiral structures is provided by the lateral assembly of helical nanofibers that provide chiral void spaces. For example, laterally grafted rodlike α-helical peptides can be aligned parallel to each other to self-assemble into 2D chiral sheet structures.[20] Considering the parallel arrangements of the helical peptides, the void spaces formed between the helical peptide arrangements are chiral and can discriminate one enantiomer from a solution of a racemic mixture. Despite such notable examples of 2D chiral materials, single-layered chiral sheets with dual chiral domains remain elusive. Here, we report single-layered chiral 2D sheet structures with dual chiral void spaces formed by chiral clusters that self-assemble with in-plane AB order in aqueous methanol solution (Figure 1). The chirality of the sheets is induced by slipped-cofacial stacks of rectangular-shaped coplanar aromatic segments with a preferred direction in clusters that are arranged laterally with up and down in-plane packing, resulting in dual chiral void spaces. Notably, the

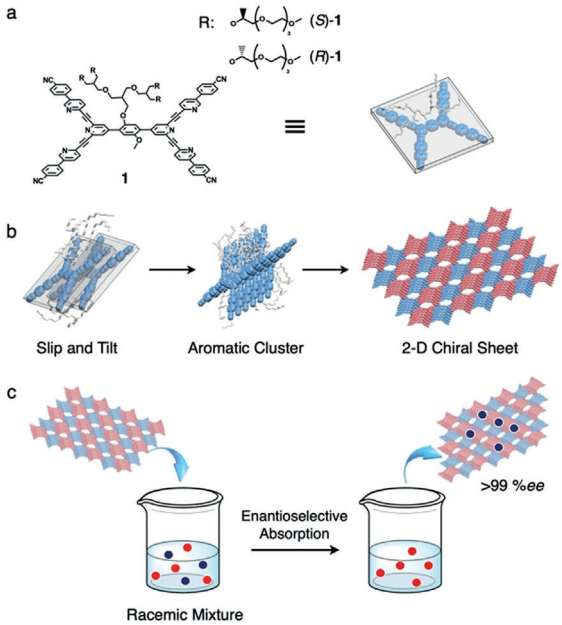

Figure 1. a) Molecular structure of **1*S***. b) Schematic representation of the formation of a single-layered chiral nanosheet structure through lateral assembly of chiral clusters consisting of slipped planar aromatic segments. c) Enantioselective absorption of the chiral sheets in a racemic mixture solution.

[*] X. Feng, B. Sun, X. Liu, Prof. M. Lee
State Key Laboratory for Supramolecular Strucuture and Materials
College of Chemistry, Jilin University
Changchun 130012 (China)
Dr. B. Shen, Prof. M. Lee
Department of Chemistry, Fudan University
Shanghai 200438 (China)
E-mail: mslee@fudan.edu.cn
Dr. J. Kim
Pohang Accelerator Laboratory, POSTECH
Pohang 37673 (Korea)
Supporting information and the ORCID identification number(s) for the author(s) of this article can be found under:
https://doi.org/10.1002/anie.202003807.

single-layered nanosheets with chiral void spaces function as highly efficient enantiomer-absorbing nanomaterials, which absorb rapidly one enantiomer from a solution of a racemic mixture with greater than 99% *ee*.

We envisioned that, when a rectangular plate-like aromatic building block is face-on grafted with a chiral flexible chain, the aromatic stack would slip in a preferred direction caused by chiral transfer to break mirror symmetry, resulting in a chiral superstructure (Figure 1b).[21–23] In this context, we synthesized a rectangular-shaped, planar aromatic segment with a hydrophilic chiral dendron at the center of the basal plane. The amphiphilic molecule **1** that forms a 2D porous structure consists of a tetrabranched aromatic segment and an internally grafted oligoether dendron. The amphiphilic molecule was synthesized from commercially available starting materials in a stepwise manner according to the procedures described in the Supporting Information. The resulting amphiphilic molecule was characterized by ^{1}H and ^{13}C NMR spectroscopy and MALDI-TOF mass spectrometry, which were shown to be in full agreement with the chemical structure presented (Figures S1 and S2).

To investigate aggregation behavior in bulk solution, we performed cryogenic transmission electron microscopy (cryo-TEM) using a frozen aqueous methanol solution (3/7, v/v) of **1**. The image shows flat 2D sheet objects with straight edges with lateral dimensions ranging from sub-micrometer to several micrometers (Figure 2a), indicating that **1** self-assembles into a 2D flat sheet structure in bulk solution. To obtain more structural information on the sheets, TEM experiments were performed with negatively stained films. The image revealed flat 2D sheet structures with straight edges (Figure 2b), consistent with the cryo-TEM result. A high-resolution image revealed 2D organized aromatic domains with an oblique lattice (Figures 2b, inset). Selected area electron diffraction (SAED) analysis showed a light spot pattern on a dark background, corresponding to an oblique lattice with in-plane dimensions of $a = 3.18$ nm and $b = 2.45$ nm, and a characteristic angle of 107° (Figure S7). Atomic force microscopy (AFM) analysis showed that the nanosheets are very flat with a uniform thickness of 2.5 nm (Figure 2c).

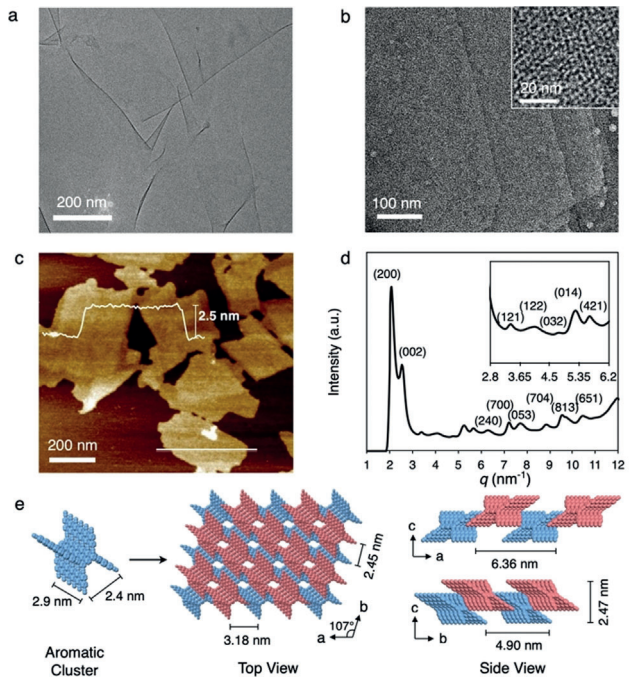

Figure 2. a) Cryo-TEM image of **1*S*** (138 μM) in aqueous methanol solution (3/7, v/v). b) Negatively stained TEM image from the cast film of **1*S***; inset: high-resolution TEM image of **1*S***. c) AFM height image of the sheets on a mica surface from evaporation of **1*S*** (46 μM) in aqueous methanol solution (3/7, v/v). The cross-sectional profile (top) is taken along the white line. d) SAXS pattern of **1*S*** with a freeze-dried sample. e) Schematic illustration of the sheet formed from lateral assembly of a cluster showing the top view (middle) and side views (right).

Considering the lattice parameters and the measured density of 1.17 g cm^{-3}, the number of molecules making up the primary structure can be calculated to be six (Table S2). When compared with the length of the diagonal aromatic axis of a molecule of **1**, the layer thickness of 2.5 nm indicates that the molecules are tilted at an angle of ≈52° with respect to the *c*-axis (Figure S8). Consequently, the tilted packing of six molecules gives rise to a discrete aromatic cluster with in-plane dimensions of 2.9 nm and 2.4 nm as a discrete primary structure of the 2D sheet assembly (Figure 2e and Figure S8). To further corroborate the primary structure of the sheets, TEM experiments were performed with a sample prepared from a highly diluted solution of **1**. TEM showed the formation of well-separated discrete nanostructures which, subsequently, self-assemble laterally into 2D planar structures at higher concentrations (Figure S9), indicating that the primary structure of the 2D sheets is a discrete aromatic cluster. This result demonstrates that the discrete clusters formed in earlier stages of the self-assembly propagate in two dimensions to form a single-layered sheet with increasing concentration (Figure 3).

The formation of the discrete clusters with the tilting of the aromatic segments in a 2D sheet arises from the tendency of rectangular plate-like aromatic blocks to form aromatic π-stacks and consequent space-filling requirements.[24]

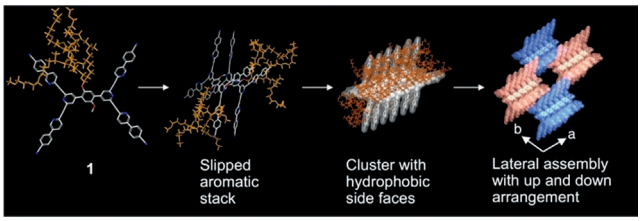

Figure 3. Schematic illustration of the self-assembly of **1** into discrete clusters consisting of six molecules with slipped packing. The clusters with hydrophobic side faces laterally associate through side-by-side hydrophobic interactions to generate a 2D sheet structure in aqueous methanol solution.

The molecular architecture comprising a planar aromatic segment and a flexible dendrimer segment drives a nanophase separation due to large chemical differences between each segment. However, fully overlapping stacks of the plate-like aromatic parts would confine grafting junctions to a flat and continuous interface with a high density of grafting sites, resulting in strong spatial crowding with chain deformation. To minimize chain deformation and fill space efficiently, the fully overlapping aromatic stacks would be broken into discrete nanostructures with slipped packings by splaying the flexible chains to provide larger interfacial area, giving rise to a chiral aromatic cluster. Indeed, when circular dichroism (CD) spectroscopy experiments were conducted with the sheet structures, the sheet solution of **1*S*** revealed a strong negative Cotton effect (Figure 4a), demonstrating that the slipped cofacial stacks of planar aromatic segments generate a chiral superstructure.[25] The sheet solution of **1*R*** formed from the enantiomer exhibits the opposite CD signal with a perfect mirror-image relationship, indicating that the chirality of the dendrimer chain is communicated to the packing of aromatic stacks to form chiral 2D sheet structures.

Based on all of our data, we propose that the slipped cofacial stacks of rectangular plate-like aromatic segments generate chiral aromatic clusters with hydrophobic side faces. Consequently, the chiral clusters hierarchically assemble through side-by-side hydrophobic interactions to form a single-layered structure, simultaneously prohibiting 3D layer stacking in aqueous methanol solution due to the hydrophilic dendrimer chains pointing in the *c*-direction of the cluster surface. Considering the shape of the cluster with protruding aromatic side parts and the lattice parameters, two-dimensional arrangements of the clusters can be illustrated by in-plane up and down ABAB order, as reflected in the SAXS pattern (Figure 2d). Taking into account that the 2D sheets of **1** consist of slipped aromatic chiral clusters with in-plane up and down AB packing, the in-plane hydrophilic dendrimer domains formed between the clusters would be alternatively arranged resulting in two different chiral spaces (Figure 4b).[21] Accordingly, we envisioned that the hydrophilic domains in an aromatic matrix can play a role as chiral containers for entrapping hydrophobic guests in a hydrophilic solvent, so that the 2D sheet with ordered chiral hydrophilic domains functions as an enantioselectively absorbing 2D material as one enantiomer would bind preferentially to the chiral void spaces.[26,27]

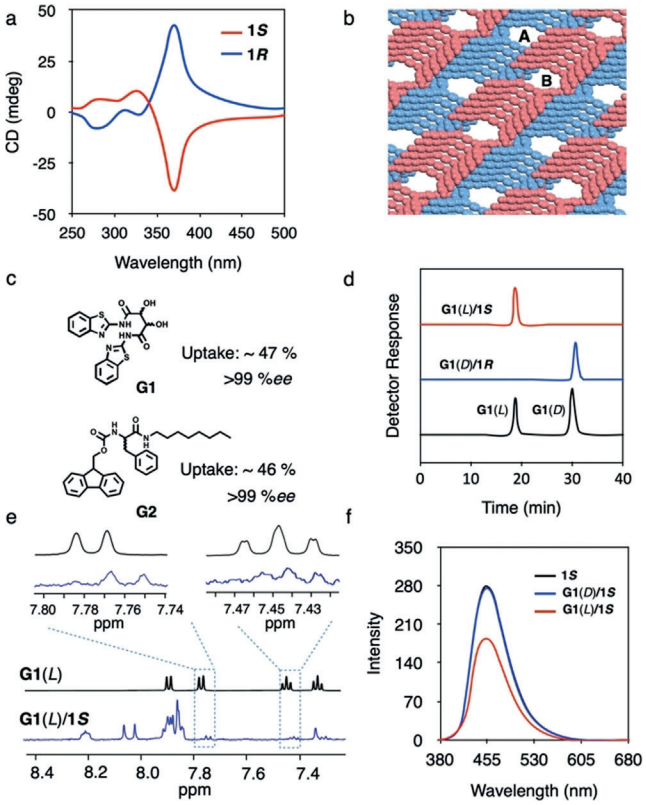

Figure 4. a) CD spectra of **1*S*** (red) and **1*R*** (blue) (46 μM) aqueous methanol solution (3/7, v/v). b) Schematic illustration of the sheet consisting of alternatively arranged A and B hydrophilic domains. c) Molecular structure of guests **G1** and **G2**. d) Chiral-HPLC traces of a racemic **G1** (black), selective uptake of the L-form by **1*S*** (red), and selective uptake of the D-form by **1*R*** (blue) in aqueous methanol solution (3/7, v/v). e) ^{1}H NMR spectra of **G1**(*L*) (42 μM) with **1*S*** (460 μM) (blue) and without **1*S*** (black) in [D_4]MeOH/[D_8]THF solution (9/1, v/v). f) Fluorescence spectra from **1*S*** (46 μM) aqueous methanol solution (3/7, v/v) with **G1**(*L*) (4.2 μM) (red), **G1**(*D*) (4.2 μM) (blue) and without guest (black).

To explore the capability of the self-assembled sheets for enantioselective absorption, we selected hydrophobically substituted tartrate (**G1**) because the void space in the aromatic sheet of **1** is bounded by hydrophobic, aromatic interior walls and the in-plane size is roughly compatible with the size of the guest in a folded conformation (Figures S8 and S11). To corroborate chiral discrimination, we added a racemic tartrate derivative (17 μM) to a solution (46 μM) of **1*S***. The internalization of the guest within the void space interior was confirmed by tracing high-performance liquid chromatography (HPLC) after the untrapped racemate had been separated from the sheet solution by gel permeation chromatography (GPC) using a Sephadex LH-20 column. Adsorption of the racemic guest by **1*S*** reached saturation after brief shaking for several minutes. We then found that the void spaces had taken up ≈47% of the tartrate guest (Figure 4c and Figure S12). This uptake result is not unexpected because the in-plane up and down arrangements of the tilted aromatic clusters generate two different chiral void spaces with non-mirror images of one another (Figure 4b). As a result, one enantiomer of **G1** fits well into only one of the two different

chiral void spaces, while it is incompatible with the other void. This was further confirmed by titration experiments using a pure **G1** enantiomer that showed 50% uptake in the pores (Figures S13 and S14).

The preferential capture of the enantiomers after saturated absorption for several minutes was then monitored by chiral HPLC. The profile showed that the peak associated with the L-enantiomer of the tartrate guest appears without any noticeable trace associated with the D-enantiomer (Figure 4d), demonstrating that the porous sheets of **1*S*** exclusively uptake the L-form with perfect inclusion preference over the D-form (>99% *ee*). Consistent with the HPLC separation result, NMR experiments showed the resonance peaks associated with the aromatic protons of the guest are upfield shifted in the range of 7.4–7.8 ppm in the sheet solution (Figure 4e), indicating that the chiral guest is entrapped in the void spaces of the sheet through host–guest aromatic interactions.[28] These aromatic interactions were further confirmed by fluorescence quenching at 450 nm upon entrapping the guests (Figure 4f). In sharp contrast, the nanosheet of **1*S*** does not exhibit apparent inclusion activity for the D-enantiomer (Figure S15), demonstrating that the enantiomer does not fit into the void spaces of **1*S***. In contrast, **1*R*** sheets uptake exclusively the D-form in the racemic tartrate solution, demonstrating that the enantioselective absorption of the sheets in a racemic mixture solution arises from the chirality of the sheet (Figure 4d).

To evaluate the enantioselectivity of the sheets with different guests, we carried out the same experiments of **1*S*** with hydrophobically substituted phenylalanine (**G2**). Similar to experiments with the tartrate derivative, the chiral sheet showed 46% uptake of **G2** and the enantioselectivity was nearly perfect (>99% *ee*) (Figures S12 and S17). The clear-cut enantioselectivity with very fast absorption in a racemic guest solution indicates that the lateral arrangement of the chiral clusters into a single layer generates two-dimensional chiral void spaces, enabling the sheets to absorb only a preferred enantiomer in a racemic mixture solution with only one discrimination event, either binding or non-binding (Figure 1c).[29] As a result, our approach can allow for the construction of superfast separation materials with perfect enantiomer selectivity. This is in great contrast to current enantioseparation materials which rely on a series of interactions between a racemic mixture and pore walls.[30–32]

In conclusion, we have constructed single-layered chiral sheet structures in aqueous MeOH solution using self-assembly of a rectangular plate-shaped aromatic amphiphile. The 2D chiral sheets consist of a lateral arrangement of chiral aromatic clusters with in-plane up and down AB order, generating dual chiral void spaces in a hydrophilic solvent. The nanosheets with chiral void spaces function as superfast enantiomer separation nanomaterials which absorb rapidly a single enantiomer in a racemic mixture with enantiomeric excess (*ee*) greater than 99%. We anticipate that our strategy to construct 2D chiral materials will provides access to porous two-dimensional materials with complex functions capable of performing multiple separations and multiple chemical reactions.

Acknowledgements

This work was supported by the National Natural Science Foundation of China (21634005 and 51473062) and Fudan Research Fund.

Conflict of interest

The authors declare no conflict of interest.

Keywords: chiral nanosheets · chiral resolution · enantiomer absorption · nanomaterials · supramolecular assembly

[1] F. Shahzad, M. Alhabeb, C. B. Hatter, B. Anasori, S. Man Hong, C. M. Koo, Y. Gogotsi, *Science* **2016**, *353*, 1137–1140.
[2] D. Sheberla, L. Sun, M. A. Blood-Forsythe, S. Er, C. R. Wade, C. K. Brozek, A. Aspuru-Guzik, M. Dincă, *J. Am. Chem. Soc.* **2014**, *136*, 8859–8862.
[3] E. Jin, M. Asada, Q. Xu, S. Dalapati, M. A. Addicoat, M. A. Brady, H. Xu, T. Nakamura, T. Heine, Q. Chen, D. Jiang, *Science* **2017**, *357*, 673–676.
[4] S. Yuan, X. Li, J. Zhu, G. Zhang, P. Van Puyvelde, B. Van der Bruggen, *Chem. Soc. Rev.* **2019**, *48*, 2665–2681.
[5] a) L. Lafferentz, V. Eberhardt, C. Dri, C. Africh, G. Comelli, F. Esch, S. Hecht, L. Grill, *Nat. Chem.* **2012**, *4*, 215–220; b) S.-Q. Xu, X. Zhang, C.-Bi. Nie, Z.-F. Pang, X.-N. Xua, X. Zhao, *Chem. Commun.* **2015**, *51*, 16417–16420; c) S. Shin, S. Lim, Y. Kim, T. Kim, T.-L. Choi, M. Lee, *J. Am. Chem. Soc.* **2013**, *135*, 2156–2159; d) K. T. Nam, S. A. Shelby, P. H. Choi, A. B. Marciel, R. Chen, L. Tan, T. K. Chu, R. A. Mesch, B.-C. Lee, M. D. Connolly, C. Kisielowski, R. N. Zuckermann, *Nat. Mater.* **2010**, *9*, 454–460; e) Y. Wang, Y. Kim, M. Lee, *Angew. Chem. Int. Ed.* **2016**, *55*, 13122–13126; *Angew. Chem.* **2016**, *128*, 13316–13320; f) S. Ghosh, D. S. Philips, A. Saeki, A. Ajayaghosh, *Adv. Mater.* **2017**, *29*, 1605408.
[6] X. Gao, Y. Zhu, D. Yi, J. Zhou, S. Zhang, C. Yin, F. Ding, S. Zhang, X. Yi, J. Wang, L. Tong, Y. Han, Z. Liu, J. Zhang, *Sci. Adv.* **2018**, *4*, eaat6378.
[7] P. Payamyar, B. T. King, H. C. Öttinger, A. D. Schlüter, *Chem. Commun.* **2016**, *52*, 18–34.
[8] J. W. Colson, A. R. Woll, A. Mukherjee, M. P. Levendorf, E. L. Spitler, V. B. Shields, M. G. Spencer, J. Park, W. R. Dichtel, *Science* **2011**, *332*, 228–231.
[9] R. Dong, M. Pfeffermann, H. Liang, Z. Zheng, X. Zhu, J. Zhang, X. Feng, *Angew. Chem. Int. Ed.* **2015**, *54*, 12058–12063; *Angew. Chem.* **2015**, *127*, 12226–12231.
[10] K.-D. Zhang, J. Tian, D. Hanifi, Y. Zhang, A. C.-H. Sue, T.-Y. Zhou, L. Zhang, X. Zhao, Y. Liu, Z.-T. Li, *J. Am. Chem. Soc.* **2013**, *135*, 17913–17918.
[11] L. Yue, S. Wang, D. Zhou, H. Zhang, B. Li, L. Wu, *Nat. Commun.* **2016**, *7*, 10742.
[12] K. Baek, I. Hwang, I. Roy, D. Shetty, K. Kim, *Acc. Chem. Res.* **2015**, *48*, 2221–2229.
[13] Y. Kim, S. Shin, T. Kim, D. Lee, C. Seok, M. Lee, *Angew. Chem. Int. Ed.* **2013**, *52*, 6426–6429; *Angew. Chem.* **2013**, *125*, 6554–6557.
[14] Y. Peng, Y. Li, Y. Ban, H. Jin, W. Jiao, X. Liu, W. Yang, *Science* **2014**, *346*, 1356–1359.
[15] S.-L. Cai, W.-G. Zhang, R. N. Zuckermann, Z.-T. Li, X. Zhao, Y. Liu, *Adv. Mater.* **2015**, *27*, 5762–5770.

[16] P. Kissel, D. J. Murray, W. J. Wulftange, V. J. Catalano, B. T. King, *Nat. Chem.* **2014**, *6*, 774 – 778.
[17] C.-J. Kim, A. Sánchez-Castillo, Z. Ziegler, Y. Ogawa, C. Noguez, J. Park, *Nat. Nanotechnol.* **2016**, *11*, 520 – 524.
[18] B. Shen, Y. Kim, M. Lee, *Adv. Mater.* **2020**, https://doi.org/10.1002/adma.201905669.
[19] B. Sun, Y. Kim, Y. Wang, H. Wang, J. Kim, X. Liu, M. Lee, *Nat. Mater.* **2018**, *17*, 599 – 604.
[20] a) X. Chen, Y. Wang, H. Wang, Y. Kim, M. Lee, *Chem. Commun.* **2017**, *53*, 10958 – 10961; b) X. Chen, Y. He, Y. Kim, M. Lee, *J. Am. Chem. Soc.* **2016**, *138*, 5773 – 5776.
[21] M. Miyata, N. Tohnai, I. Hisaki, T. Sasaki, *Symmetry* **2015**, *7*, 1914 – 1928.
[22] T. Kajitani, K. Motokawa, A. Kosaka, Y. Shoji, R. Haruki, D. Hashizume, T. Hikima, M. Takata, K. Yazawa, K. Morishima, M. Shibayama, T. Fukushima, *Nat. Mater.* **2019**, *18*, 266 – 272.
[23] Y. Wang, J. Xu, Y. Wang, H. Chen, *Chem. Soc. Rev.* **2013**, *42*, 2930 – 2962.
[24] M. Lee, B.-K. Cho, Y.-G. Jang, W.-C. Zin, *J. Am. Chem. Soc.* **2000**, *122*, 7449 – 7455.
[25] a) A. Raudino, M. Pannuzzo, *J. Chem. Phys.* **2012**, *137*, 134902; b) Y. Kim, J. Kang, B. Shen, Y. Wang, Y. He, M. Lee, *Nat. Commun.* **2015**, *6*, 8650; c) M. Morisue, H. Fukui, M. Shimizu, K. Inoshita, Y. Morisaki, Y. Chujo, *Tetrahedron Lett.* **2014**, *55*, 271 – 274.
[26] L. Chen, P. S. Reiss, S. Y. Chong, D. Holden, K. E. Jelfs, T. Hasell, M. A. Little, A. Kewley, M. E. Briggs, A. Stephenson, K. M. Thomas, J. A. Armstrong, J. Bell, J. Busto, R. Noel, J. Liu, D. M. Strachan, P. K. Thallapally, A. I. Cooper, *Nat. Mater.* **2014**, *13*, 954 – 960.
[27] Y. Peng, T. Gong, K. Zhang, X. Lin, Y. Liu, J. Jiang, Y. Cui, *Nat. Commun.* **2014**, *5*, 4406.
[28] a) J. S. Mugridge, R. G. Bergman, K. N. Raymond, *J. Am. Chem. Soc.* **2011**, *133*, 11205 – 11212; b) A. S. Shetty, J. Zhang, J. S. Moore, *J. Am. Chem. Soc.* **1996**, *118*, 1019 – 1027.
[29] A. W. Hauser, N. Mardirossian, J. A. Panetier, M. Head-Gordon, A. T. Bell, P. Schwerdtfeger, *Angew. Chem. Int. Ed.* **2014**, *53*, 9957 – 9960; *Angew. Chem.* **2014**, *126*, 10117 – 10120.
[30] R. Xie, L.-Y. Chu, J.-G. Deng, *Chem. Soc. Rev.* **2008**, *37*, 1243 – 1263.
[31] M. N. Corella-Ochoa, J. B. Tapia, H. N. Rubin, V. Lillo, J. González-Cobos, J. L. Núñez-Rico, S. R. G. Balestra, N. Almora-Barrios, M. Lledós, A. Güell-Bara, J. Cabezas-Giménez, E. C. Escudero-Adán, A. Vidal-Ferran, S. Calero, M. Reynolds, C. Martí-Gastaldo, J. R. Galán-Mascarós, *J. Am. Chem. Soc.* **2019**, *141*, 14306 – 14316.
[32] X. Han, J. Huang, C. Yuan, Y. Liu, Y. Cui, *J. Am. Chem. Soc.* **2018**, *140*, 892 – 895.

Manuscript received: March 13, 2020
Accepted manuscript online: April 4, 2020
Version of record online: ■■ ■■, ■■■■

Communications

Chiral Resolution

X. Feng, B. Shen, B. Sun, J. Kim, X. Liu, M. Lee* ——— ■■■■–■■■■

Single-Layered Chiral Nanosheets with Dual Chiral Void Spaces for Highly Efficient Enantiomer Absorption

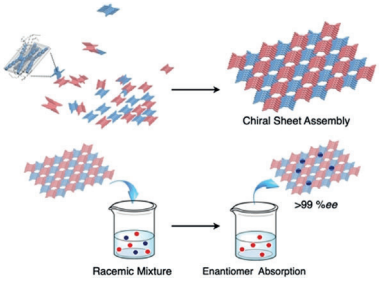

Being picky: Single-layered chiral 2D sheet structures with dual chiral void spaces are formed in aqueous methanol solution from discrete clusters of planar aromatic segments with in-plane up and down AB packing. The slipped cofacial stacks of aromatic segments induce the chirality of the sheet. The nanosheets absorb rapidly one enantiomer from a solution of the racemic mixture with greater than 99% *ee*.